ISSN: 0973-3469, Vol.17, No.(1) 2020, Pg. 34-46

Material Science Research India

www.materialsciencejournal.org

Structural and Magnetic Properties of $Ba_{1-x}Re_xCo_2Zn_xFe_{16-x}O_{27}$ W-type Hexaferrite Prepared by Ball Milling Method

MOHAMMAD K. DMOUR[1], EMAN S. AL-HWAITAT[1], IBRAHIM BSOUL[2] and SAMI H. MAHMOOD[1,3]*

[1]Physics Department, The University of Jordan, Amman 11942, Jordan.
[2]Physics Department, Al al-Bayt University, Mafraq 13040, Jordan.
[3]Department of Physics and Astronomy, Michigan State University, East Lansing, MI 48824, USA.

Abstract

Rare earth substituted W-type hexaferrites were prepared by mixing and ball milling starting powders with molar ratios consistent with the stoichiometry of $Ba_{1-x}Re_xCo_2Zn_xFe_{16-x}O_{27}$ (Re is a rare-earth element; x = 0.1 and 0.2), pelletizing, and sintering 1300°C. X-ray diffraction patterns showed a pure W-type phase in all samples, except in the Nd-Zn (x = 0.1) substituted sample which revealed the presence of an impurity α-Fe_2O_3 nonmagnetic phase. The crystallization of the W-type phase in all samples was further confirmed by the characteristic Curie temperature ranging between 476°C and 484°C as revealed by the thermomagnetic measurements. Scanning electron microscopy imaging revealed the variations of the particle size and morphology, and porosity of the prepared samples. The magnetic measurements indicated that the RE–Zn substitution improved the saturation magnetization slightly relative to the un-substituted Co2W hexaferrite, and resulted in a decrease of the coercivity and magnetocrystalline anisotropy field. In addition, the peaks below 300°C in the thermomagnetic curves is an indication of the occurrence of spin reorientation transitions in the prepared hexaferrites.

Article History

Received: 7 December 2019
Accepted: 21 January 2020

Keywords:

Magnetic properties;
Structural properties;
Spin reorientation transition;
W-type hexaferrites.

Introduction

Hexagonal ferrites (hexaferrites) belonging to an important class of magnetic oxides were discovered in the 1950s, and demonstrated high potential for important practical applications with economic feasibility, which led to an increasing interest in the production and characterization of these materials. The major utilization of hexaferrites is in the production of permanent magnets, as well as a wide range of applications including magnetic

CONTACT Sami H. Mahmood s.mahmood@ju.edu.jo Physics Department, The University of Jordan, Amman 11942, Jordan.

Doi: http://dx.doi.org/10.13005/msri/170106

recording and electrical devices operating in the GHz frequency range.[1-6] The employment of hexaferrites in a plethora of magnetic material applications was further encouraged by their favourable properties, chemical stability, relatively high operating temperature, and cost effectiveness.[7-12]

The various members of the hexagonal ferrite family (M-, Y-, W-, Z-, X-, and U-type) exhibit different magnetic properties, which facilitated their potential use for a variety of applications.[13, 14] The molecular formula of the W-type hexaferrite ($BaMe_2Fe_{16}O_{27}$) can be viewed as a superposition of M-type hexaferrite ($BaFe_{12}O_{19}$) and spinel (S) structural block (W = M + S; S = $Me_2Fe_4O_8$).[15, 16] In the case of Me = Co, the saturation magnetization of the spinel phase is higher than that of the M-type hexaferrite,[13] which explains the higher saturation magnetization of the W-type hexaferrite compared with the M-type. The unit cell of the W-type structure contains two Co_2W molecules in the alternate stacking SSRS*S*R* of the R ($BaFe_6O_{11}$) and S structural blocks (the star means rotation of the block around the *c*-axis by 180º).[15, 17]

W-type hexaferrite was recognized as a soft magnetic material with potential importance for microwave absorption.[18-23] The microwave properties of the W-type phase were improved by cationic substitutions, such as the partial substitution of Ba^{2+} ions by Er^{3+}, Sm^{3+}, and Nd^{3+}.[15, 23, 24] Also, partial substitution of Dy^{3+} for Fe^{3+} in Ni_2W hexaferrites,[21] and La-Ni substitution in Co_2W,[25] have shown promising modifications for microwave absorption applications in the GHz range. However, adequate structural and magnetic characterization of these materials remain limited in the literature.

The magnetic structure of Co_2W hexaferrites was investigated by Mössbauer spectroscopy and neutron diffraction. Mössbauer results revealed spin reorientation transition from planer anisotropy to conical spin structure with vertex angle of 50º to the *c*-axis at 242ºC; this angle remained constant up to the maximum temperature of 272ºC used in the study,[26] where additional spin reorientation transition to axial spin configuration (parallel to the *c*-axis) could occur at higher temperatures. The spin reorientation transition temperature was reported to decrease with the decrease of Co content in $(Zn,Co)_2$-W hexaferrites,[26, 27] exhibiting a maximum value for the Co_2W end compound. This result was further supported by previous results based on magnetic data on $BaCo_{0.62}Zn_{1.38}Fe_{16}O_{27}$, which indicated that the compound is planer up to – 68ºC, at which temperature it undergoes spin reorientation to axial spin structure parallel to the *c*-axis[28] On the other hand, Neutron diffraction study revealed conical spin structure with angle of 70º to the *c*-axis up to 180ºC, after which the angle decreased and the spin structure becomes axial (parallel to the *c*-axis) at 280ºC.[29] Among other reasons, the seemingly conflicting reported results could be due to differences in sample preparation, types of measurements adopted, or experimental uncertainties. The present study is concerned with the synthesis of pure RE-substituted Co_2W hexaferrites. The synthesized hexaferrites were examined by means of structural and magnetic characterization techniques, and the effects of RE substitution were investigated. This article is extracted from the unpublished Ph.D. thesis of M. K. Dmour, where the corresponding section in the thesis was written and organized in a format ready for publication. All samples in this work were prepared by Dmour, but the measurements and data analysis were partly contributed by others, who were included in the list of coauthors.

Experimental Techniques

We prepared $Ba_{1-x}Re_xCo_2Zn_xFe_{16-x}O_{27}$ (Re = La, Nd, Pr; x = 0.1, 0.2) hexaferrites by mixing stoichiometric ratios of high purity (> 99%) $BaCO_3$, Fe_2O_3, ZnO, and Re_2O_3 (Sigma-Aldrich made), and ball milling by Fritch Pulveressette-7 ball mill for 16 h. The milling was performed using zirconia bowls and balls; the powder to ball ratio was 1:12. Then pellets of 12.5 mm in diameter were made from the powder mixtures by compressing under a force of 50 kN, and subsequently sintering in air at 1300°C for 2 h.

X-ray powder diffraction (XRD) was employed to examine the structural characteristics of the prepared samples using a 7000-Shimadzu X-Ray Diffractometer (λ = 0.15406 nm). The refined structural parameters were obtained from the results of Rietveld analysis of the diffraction data using FullProf software. The particle size and surface morphology in the samples were investigated by scanning electron microscopy (SEM). The room

temperature magnetic data were obtained by performing magnetic measurements on the samples using a commercial vibrating sample magnetometer (VSM).

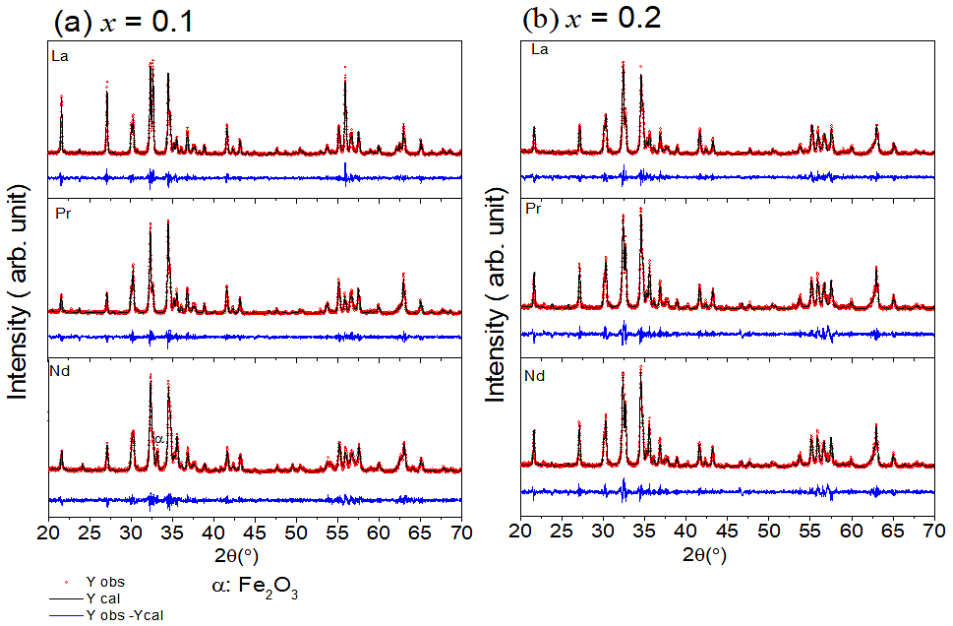

Fig. 1: Rietveld refinement of the XRD patterns of RE – Zn substituted Co_2W samples. The peak labeled by (α) corresponds to an impurity α-Fe_2O_3 oxide phase

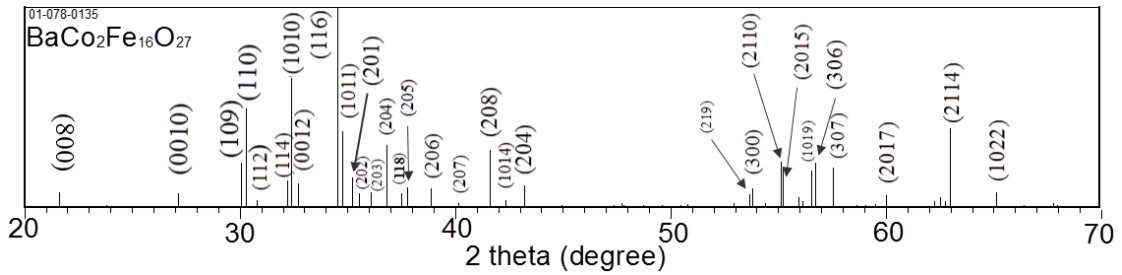

Fig. 2: The standard pattern (JCPDS: 01-078-0135) of Co_2W hexaferrite, with Miller indices of the reflections indicated

Results and Discussion

XRD Results

The diffraction pattern of $BaCo_2Fe_{16}O_{27}$ (x = 0.0) sample was reported in a recent publication,[30] where pure Co_2W phase was obtained. Fig.1 shows Rietveld analysis of the diffraction patterns of the samples $Ba_{1-x}Re_xCo_2Zn_xFe_{16-x}O_{27}$ (Re = La, Nd, and Pr; x = 0.1, 0.2), which indicated that all samples, except the (Nd-Zn; x = 0.1) sample, consisted of a pure Co_2W hexaferrite phase whose peak positions agree with the standard pattern (JCPDS file #: 01-078-0135) shown in Fig. 2. The relative intensities of the (00*l*) reflections, however, are clearly enhanced compared with those of the standard pattern. The observed enhancement of the relative intensity of these reflections, especially for the sample with La-Zn substitution (x = 0.1), is consistent with previously reported structural texture along the *c*-axis in Ga-substituted Co_2W hexaferrites.[30] Fig. 3 shows a representative plot

showing the main structural peaks of the sample with La-Zn substitution (x = 0.1) in the angular range $2\theta = 30^{\circ}$ to 38°, which demonstrated a perfect match between the experimental peak positions and those of the standard pattern (shown in bars representing the intensities of the reflections). In this figure, the enhancement of the relative intensity of the (0012) reflection is obvious. Further, the pattern of the Nd-Zn substituted sample revealed the presence of a minor α-Fe_2O_3 oxide phase as indicated by the main structural peak (labeled α) of this phase. Fig. 4 shows a match between the experimental peaks and those of the standard pattern, with a small peak corresponding to the minor α-Fe_2O_3 phase. In a previous study, the presence of a secondary cubic $CoFe_2O_4$ spinel phase in Co_2W hexaferrites was reported,[31] whereas α-Fe_2O_3 impurity phase was reported to occur in other types of hexaferrites.[18, 32-34]

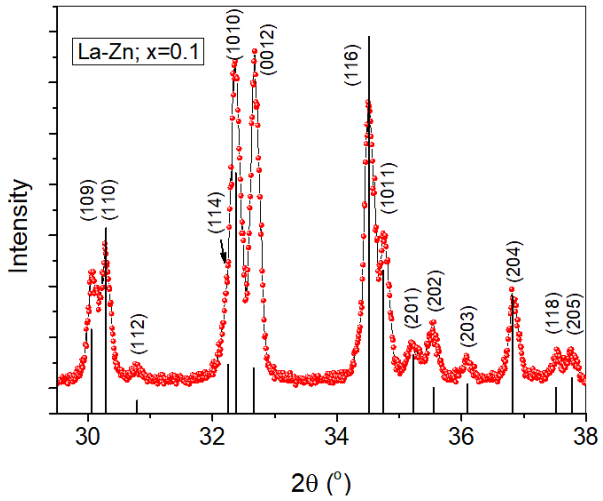

Fig. 3: Main structural peaks of La – Zn substituted Co2W sample (points) and corresponding peaks of the standard pattern (bars)

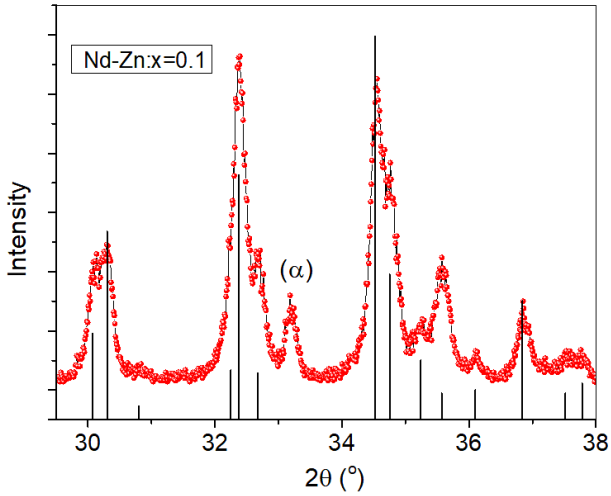

Fig. 4: Main structural peaks of Nd – Zn substituted Co_2W sample (points) and corresponding peaks of the standard pattern (bars). The peak labeled by (α) corresponds to an impurity α-Fe_2O_3 oxide phase

Rietveld analysis facilitates determination of the refined structural parameters of the structural phases in the samples; the results are shown in Table 1. The results indicated that the lattice parameter a = 5.90 Å for the W-type phase was the same in all samples and agreed with published data for the unsubstituted Co_2W.[16, 30, 35] The observed values of the lattice constant c, however, were in general slightly lower, owing to the smaller ionic radii of the substituted RE ions in comparison with Ba^{2+}.[36] The lattice parameter c fluctuated slightly (0.09%) around the average value of 32.89 Å, and the cell volume fluctuated slightly (0.16%) around the average value of 991.6 Å^3. Evidently, the structural parameters did not increase with the substitution of Zn^{2+} ions having higher ionic radius compared with Fe^{3+} ions, and the effect of RE substitution was dominant. This could be due to the substitution of a relatively large fraction of Ba^{2+} by RE^{3+} (10% or 20%) at substitutional positions in the oxygen layers, whereas only 0.625% or 1.25% of the Fe^{3+} ions were substituted by Zn^{2+} ions at interstitial sites.

Table 1: Lattice parameters, cell volume, and X-ray density of $Ba_{1-x}Re_xCo_2Zn_xFe_{16-x}O_{27}$ samples

RE	*x*	phase	*a* (Å)	*c* (Å)	*V* (Å^3)	ρ_x(g/cm^3)	ρ_b(g/cm^3)
La	0.1	W	5.90	32.88	991.5	5.30	4.87
	0.2	W	5.90	32.87	990.7	5.30	4.75
Pr	0.1	W	5.90	32.90	992.4	5.29	4.71
	0.2	W	5.90	32.90	991.8	5.29	4.57
Nd	0.1	W	5.90	32.87	990.0	5.30	4.09
		α- Fe_2O_3	5.03	13.75	301.3		
	0.2	W	5.90	32.92	992.9	5.28	4.62

The X-ray density of the W-type phase was calculated from the molecular mass and the refined cell volume, and the bulk density was measured using Archimedes principle; the results are also listed in Table 1. The constancy of the refined X-ray density (5.29 ± 0.01 g/cm^3) could be due to the small changes of the molecular mass and cell volume with the RE-Zn substitution. Comparison between the measured bulk density and theoretical x-ray density indicated that all pure W-type hexaferrites possess relatively high density, reaching 86.3% – 91.9% of the theoretical density. The lowest bulk density of 77.2% for the Nd–Zn substituted sample with x = 0.1 is also relatively high.

Stokes and Wilson formula was used to calculate the crystallite size (D) of each sample using the corrected integral breadth (βc) of a given XRD peak, where[33, 37, 38]

$$D=(\lambda)/(\beta c \cos\theta) \quad ...(1)$$

The instrumental broadening was estimated by the breadth of standard Si reflections, whereas the observed integral breadth of a given reflection in the patterns of the samples was determined from the integrated intensity (area A) and the maximum peak intensity (I_0) in accordance with the relation:

$$\beta=A/I_0 \quad ...(2)$$

The average crystallite size was determined from the (0010) reflection at 2θ = 27.11° and the (110) reflection at 2θ = 30.27°, and the results for the size parallel to the c-axis and in the hexagonal plane, respectively, are listed in Table 2. The crystallite size along the c-axis for the sample with (La–Zn; x = 0.1) substitution was 351 nm, which is significantly larger than that for the other samples,

where the sizes fluctuated in the range of ~ 110 to 200 nm. This result is consistent with the highest observed bulk density (91.9% of the theoretical density) for this sample. Generally speaking, the crystallite size of all samples is higher than the range of applicability (~ 100 nm) of the technique.[37] However, the results could indicate that the lowest crystallite size (~110 nm) of Nd–Zn substituted sample with x = 0.1 could be associated with the lowest observed bulk density for this sample.

Table 2: The crystallite size of the W-type phase along the c-axis and in the hexagonal plane

RE/*x*	*D* (nm)	
	Parallel to the *c*-axis (0010)	**Parallel to the hexagonal plane (110)**
La/0.1	351	192
La/0.2	161	138
Pr/0.1	197	205
Pr/0.2	177	134
Nd/0.1	112	108
Nd/0.2	177	113

SEM Results

Figures 5 to 8 show representative SEM images of all samples. The image in Fig. 5 (a) for the sample with La–Zn substation (x = 0.1) revealed crystallization of large (> 2 μm), perfect hexagonal platelets with step-like formation indicative of topotactical grain growth.[30] The closely-packed plates with no obvious porosity is consistent with the high bulk density of this sample, and the stacking of the hexagonal plates along the *c*-axis is consistent with the highest degree of structural texture along the *c*-axis as revealed by the relative peak intensities in the XRD pattern. However, the image of the sample with x = 0.2 revealed the presence of closely-packed, randomly oriented sharp-edged particles with typical size of ~ 2 μm (Fig. 5 (b)).

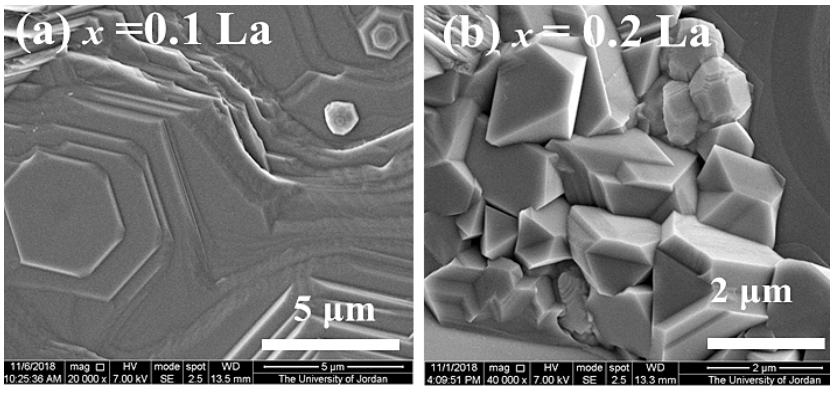

Fig. 5: Representative SEM images of the samples with La-Zn substitution (a) x = 0.1 and (b) x = 0.2

Fig. 6 shows representative SEM images of the sample with Pr–Zn substation (x = 0.1). The images show the presence hexagonal particles with in-plane size of ~ 1 – 2 μm in some regions of the sample (Fig.6 (a)), in addition to large non-particulate porous structure with hexagonal pores

(Fig.6 (b)). The hexagonal pores revealed the internal crystallographic hexagonal structure in the large non-particulate mass.

Fig. 7 shows representative images of the sample with Pr-Zn substitution (x = 0.2). Some relatively small hexagonal plates few microns in diameter were observed, although the majority of the sample consisted of large, porous non-particulate masses (Fig.7 (b)). This porosity is associated with the relatively low bulk density of this sample compared to other samples.

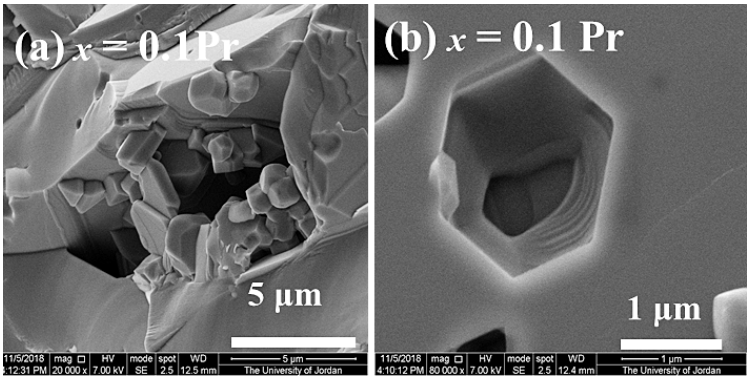

Fig. 6: Representative SEM images of the sample with Pr-Zn substitution (x = 0.1)

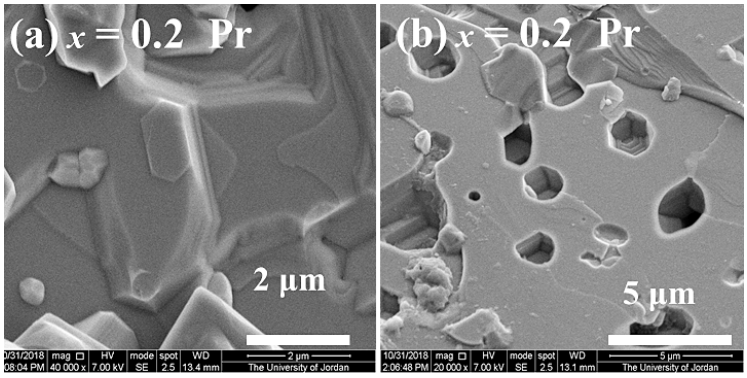

Fig. 7: Representative SEM images of the sample with Pr-Zn substitution (x = 0.2)

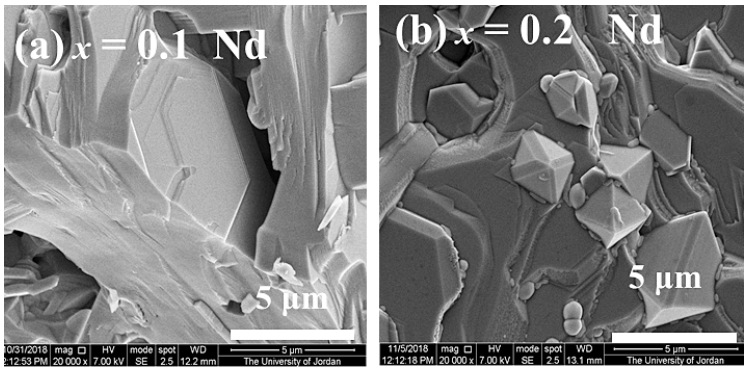

Fig. 8: Representative SEM images of the sample with Nd-Zn substitution (a) x = 0.1 and (b) x = 0.2

Further, representative images of the sample with Nd–Zn substitution (Fig. 8) indicated crystallization of large hexagonal plates (> 5 μm) with step-like formation. However, a small fraction of smaller particles was observed in Fig. 8 (b) at x = 0.2.

Magnetic Measurements

Isothermal Magnetization

Magnetic hysteresis measurements in the field range ± 10 kOe were carried out on all samples, and revealed characteristics of relatively soft magnetic materials. However, for the sake of clarity, the loops in the field range of ± 2 kOe were presented in Fig. 9. These curves were used to determine the remnant magnetization and coercivity for each sample. On the other hand, the saturation magnetization (M_s) was estimated from the behaviour of the magnetization curve in the high-field range (8.0 – 10.0 kOe) by employing the law of approach to saturation[39]

$$M=M_s\,(1-A/H-B/H^2)+\chi H \qquad ...(3)$$

Although this equation included the contributions from crystal imperfections (represented by the constant *A*), magnetocrystalline anisotropy (represented by the constant *B*), and forced magnetization (χH), the linear behaviour of *M* vs. $1/H^2$ indicated clearly that the magnetization behavior in the high-field range was dominated by the high magnetocrystalline anisotropy of the ferrites, and that other contributions were negligible. By fitting the linear relation with the best straight line, the saturation magnetization (intercept of the line with the *M*-axis) was determined. The slope of the straight line was used to determine the the anisotropy field (H_a) using the relation[40]

$$B = \frac{H_a^2}{15} \qquad ...(4)$$

The results of the analysis of the hysteresis data in Table 3 revealed a 15% to 30% improvement of the saturation magnetization relative to Co_2W hexaferrites prepared by coprecipitation,[41-43] and the sample with La-Zn (x = 0.2) substitution exhibited the highest value of 78.0 emu/g. The lower value of 74.6 emu/g for La–Zn substitution with x = 0.1 was higher than that of the recently reported value of 70.22 emu/g for $Ba_{0.9}La_{0.1}Fe_2^{2+}Fe_{16}^{3+}O_{27}$.[44] On the other hand, the samples with Nd–Zn substitutions exhibited the lowest values of the saturation magnetization (71.9 to 73.2 emu/g) compared with the other substitutions; these values are still in good agreement with those of Co_2W.[30, 45] The increase of the saturation magnetization with RE–Zn substitution could be due to the preferential substitution of Fe^{3+} ions by nonmagnetic Zn^{2+} ions at spin-down sites.

Table 3: Saturation magnetization (M_s), remanence (M_r), coercive field (Hc), and anisotropy field (H_a) for $Ba_{1-x}Re_xCo_2Zn_xFe_{16-x}O_{27}$ hexaferrites

RE	*x*	M_s (*(emu/g)*	M_r*(emu/g)*	Hc (Oe)	H_a(kOe)
La	0.1	74.6	1.80	33	8.27
	0.2	78.0	4.69	49	8.64
Pr	0.1	75.9	3.41	51	7.83
	0.2	73.5	2.92	52	7.46
Nd	0.1	73.2	6.11	88	6.39
	0.2	71.9	3.66	68	7.83

The coercivity of all samples was somewhat below the value of 90 Oe for $BaCo_2Fe_{16}O_{27}$ prepared by a similar method,[16, 30] and the samples with Nd-Zn substitution exhibited the highest values of 88 Oe and 68 Oe. The coercivity for the rest of the samples was below these values, and the lowest coercivity of 33 Oe was observed for La–Zn (x = 0.1) sample. These values are to be compared with those for Co_2W hexaferrites prepared by a different method (coprecipitation), which exhibited much higher values.[42, 43] The observed differences of the coercivity could be due to differences in the preparation method

and experimental conditions, leading to different microstructures which play a key role in the coercivity.

To examine the correctness of the interpretation provided in the last sentence, we must simultaneously investigate the behavior of the anisotropy field (H_a) with RE-Zn substitution, since it is known that changes in H_a play an important role in changing the coercivity. Table 3 shows that the values of H_a of all samples were in the range of 6.39 – 8.64 kOe, in agreement with the values for pure Co_2W samples[16,30] However, the sample with Nd-Zn substitution (x = 0.1) exhibited the lowest value of 6.39 kOe, whereas this same sample exhibited the highest coercivity. Also, the sample with La-Zn substitution (x = 0.1) exhibited the lowest coercivity of 33 Oe, whereas its anisotropy field is one of the highest in the measured samples. This could be an indication that the observed fluctuations in the coercivity are more likely to be of microstructural origin rather than magnetocrystalline origin.

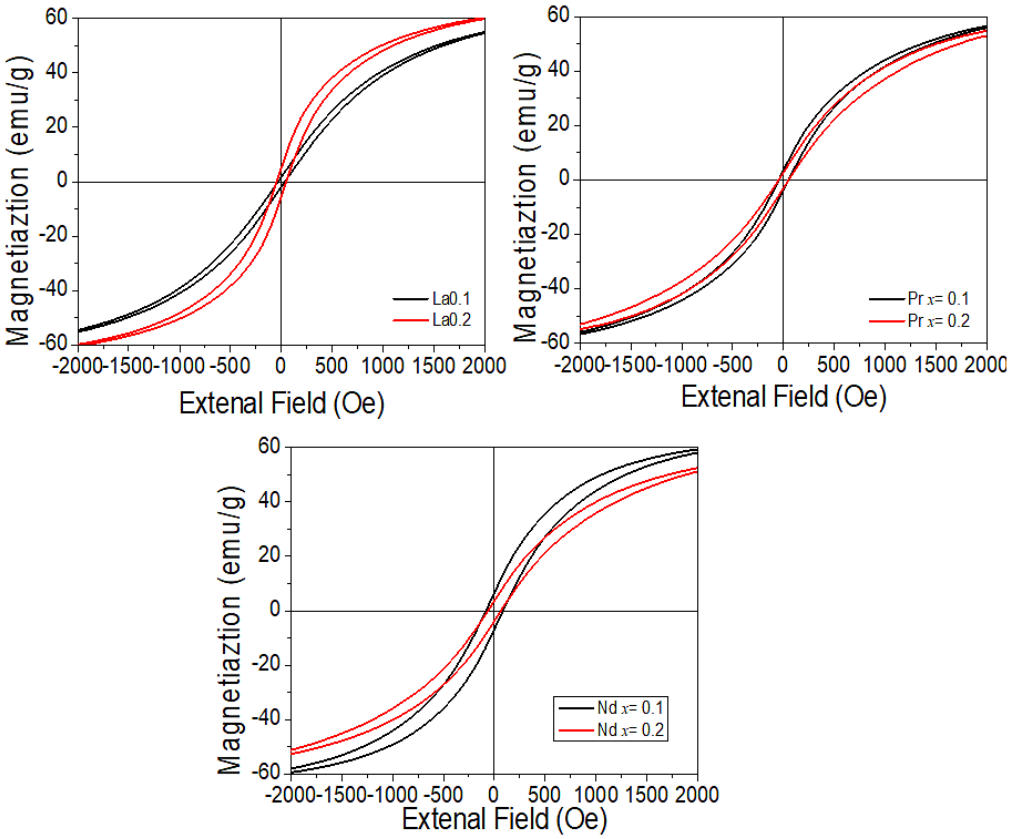

Fig. 9: Expanded view of the hysteresis loops of the RE–Zn substituted Co_2W hexaferrites

Thermomagnetic Measurements

The behavior of the magnetization at a constants field of 100 Oe with increasing temperature was investigated for all samples, and the results are shown in Fig. 10. The curves indicated that all samples went through magnetic phase transitions at different temperatures. All thermomagnetic curves exhibited a peak below 300ºC. The initial increase of the magnetization is associated with spin reorientation transition common to Co-containing W-type phase,[16, 30] and the peak occurs as a result of competition with thermal effects. At higher temperatures (> 450°C), the magnetization dropped sharply as a consequence of ferromagnetic-to-paramagnetic phase transitions. The derivative of the magnetization with respect to temperature (d*M*/d*T*)

exhibited a sharp (negative) peak at the transition temperature, from which the Curie temperature of the magnetic phase was determined (Table 4). The transition temperature obtained from the strong peak in the range 476 – 484°C is associated with the Curie temperature (T_c) of the W-type phase. These value of Curie did not change appreciably from the values previously reported for Co_2W hexaferrite.[26, 30] A second weak peak in the derivative curves was observed at higher temperatures (534 – 539°C). Since the structural analysis did not show secondary phases (except for the sample with Nd-Zn substitution with x = 0.1), this weak peak can be attributed to the enhancement of the superexchange interactions strength in Co-rich regions of the samples. Similar secondary step reduction of the magnetization was observed in the thermomagnetic curves of Co-containing M-type,[46] Y-type,[47] and W-type hexaferrites.[16, 30]

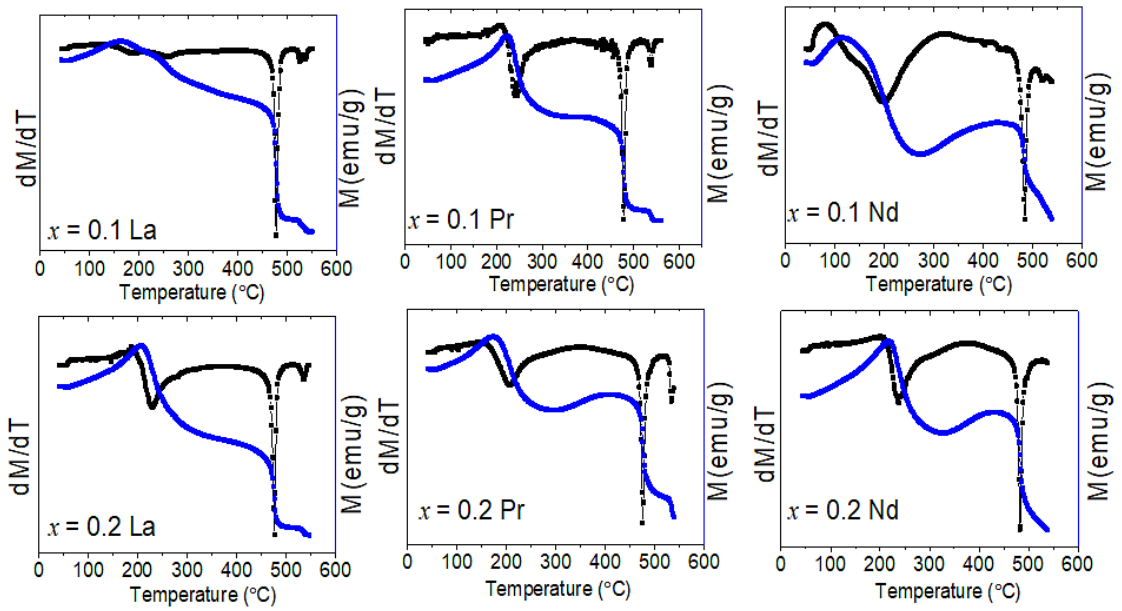

Fig. 10: Thermomagnetic curves at an applied field of 100 Oe (blue curves), and their derivatives (black curves) for all samples

Table 4: Curie temperatures of the magnetic phases in the samples

RE/x	T_c (º C)	
La/0.1	477	534
La/0.2	476	535
Pr/0.1	478	539
Pr/0.2	476	535
Nd/0.1	484	-
Nd/0.2	484	-

Conclusion

Highly pure W-type hexaferrites $Ba_{1-x}Re_xCo_2Zn_xFe_{16-x}O_{27}$ with RE-Zn substitutions were successfully produced by ball milling stoichiometric ratios of the starting powders and sintering at 1300°C. The physical particle size revealed by SEM imaging was found to be large, and the crystallite size determined from analysis of the XRD patterns was found to be > 100 nm for all samples, indicating a high degree of crystallization of highly dense RE–Zn substituted W-type pellets. The saturation magnetization improved with RE–Zn substitution compared with the

unsubstituted Co_2W, while the coercivity remained below 100 Oe for all samples. The thermomagnetic curves confirmed the phase purity, and revealed the Curie temperature of the magnetic phases. The Curie temperature was not influenced significantly by the RE-Zn substitution, and spin reorientation transitions were observed in the temperature range < 300ºC for all samples, rendering these materials of potential importance for magnetic refrigeration applications.

Acknowledgement
M.K. Dmour would like to dedicate his work to the soul of his late mother (Salha Dmour). S.H. Mahmood is thankful to The University of Jordan for providing the necessary support during his sabbatical leave at Michigan State University, East Lansing, MI, USA.

Funding
There is no special funding for this particular work.

Conflict of Interest
The authors have no conflicts of interest to disclose

References

1. S.R. Ejaz, M.A. Khan, M.F. Warsi, M.N. Akhtar, A. Hussain, Study of structural transformation and hysteresis behavior of Mg-Sr substituted X-type hexaferrites, *Ceramics International,* 44 (2018) 18903-18912.
2. B. Ul-ain, A. Zafar, S. Ahmed, To explore a new class of material (X-type hexaferrites) for N_2O decomposition, *Catalysis Science & Technology*, 5 (2015) 1076-1083.
3. Abdul Majeed, Muhammad A. Akhtar, Faseeh ur Raheem, Altaf Hussain, F. Iqbal, Ghulam Murtaza, Majid N. Akhtar, Imran Shakir, M.F. Warsi, Structural elucidation and magnetic behavior evaluation of rare earth (La, Nd, Gd, Tb, Dy) doped BaCoNi-X hexagonal nanosized ferrites, *Journal of Magnetism and Magnetic Materials*, 408 (2016) 147-151.
4. A. Kagdi, N. Solanki, R.B. Jotania, Effect of sintering temperature on structural property of X-type barium-zinc hexaferrites, AIP Conference Proceedings, AIP Publishing, 2016, pp. 020046.
5. A.R. Kagdi, N.P. Solanki, F.E. Carvalho, S.S. Meena, P. Bhatt, R.C. Pullar, R.B. Jotania, Influence of Mg substitution on structural, magnetic and dielectric properties of X-type barium-zinc hexaferrites $Ba_2Zn_{2-x}Mg_xFe_{28}O_{46}$, *Journal of Alloys and Compounds*, 741 (2018) 377-391.
6. Y. Wu, Y. Huang, L. Niu, Y. Zhang, Y. Li, X. Wang, Pr^{3+}-substituted W-type barium ferrite: Preparation and electromagnetic properties, *Journal of Magnetism and Magnetic Materials*, 324 (2012) 616-621.
7. R.C. Pullar, Hexagonal ferrites: a review of the synthesis, properties and applications of hexaferrite ceramics, *Progress in Materials Science*, 57 (2012) 1191-1334.
8. V.G. Harris, A. Geiler, Y. Chen, S.D. Yoon, M. Wu, A. Yang, Z. Chen, P. He, P.V. Parimi, X. Zuo, Recent advances in processing and applications of microwave ferrites, *Journal of Magnetism and Magnetic Materials,* 321 (2009) 2035-2047.
9. S.H. Mahmood, Ferrites with High Magnetic Parameters, in: S.H. Mahmood, I. Abu-Aljarayesh (Eds.) Hexaferrite Permanent Magnetic Materials, *Materials Research Forum LLC, Millersville,* PA, 2016, pp. 111-152.
10. S.H. Mahmood, High Performance Permanent Magnets, in: S.H. Mahmood, I. Abu-Aljarayesh (Eds.) Hexaferrite Permanent Magnetic Materials, Materials Research Forum LLC, Millersville, PA, 2016, pp. 47-73.
11. I. Abu-Aljarayesh, Magnetic Recording, in: S.H. Mahmood, I. Abu-Aljarayesh (Eds.) Hexaferrite Permanent Magnetic Materials, Materials Research Forum LLC, Millersville, PA, 2016, pp. 166-181.
12. S.H. Mahmood, Permanent Magnet Applications, in: S.H. Mahmood, I. Abu-Aljarayesh (Eds.) Hexaferrite Permanent Magnetic Materials, Materials Research Forum LLC, Millersville, PA, 2016, pp. 153-165.
13. J. Smit, H.P.J. Wijn, Ferrites, Wiley, New York, 1959.
14. S. Chikazumi, Physics of Ferromagnetism 2e, 2nd ed., Oxford University Press Oxford, 2009.
15. J. Xu, H. Zou, H. Li, G. Li, S. Gan, G. Hong, Influence of Nd^{3+} substitution on the

microstructure and electromagnetic properties of barium W-type hexaferrite, *Journal of Alloys and Compounds,* 490 (2010) 552-556.

16. S.H. Mahmood, Q. Al-Shiab, I. Bsoul, Y. Maswadeh, A. Awadallah, Structural and magnetic properties of $(Mg, Co)_2W$ hexaferrites, arXiv preprint arXiv:1711.08581, (2017).
17. J. Tang, X. Liu, K.M.U. Rehman, D. Li, M. Li, Y. Yang, Microstructure and characterization of W-type hexaferrite $Ba_{1-x}La_xFe_2^{2}+Fe_{16}^{3}+O_{27}$ prepared by solid state method, *Journal of Magnetism and Magnetic Materials*, 452 (2018) 354-359.
18. Hua Zou, Shuhuan Li, Liqun Zhang, Shani Yan, Hanguang Wu, Shuai Zhang, M. Tian, Determining factors for high performance silicon rubber microwave absorbing materials, *Journal of Magnetism and Magnetic Materials*, 323 (2011) 1643-1651.
19. Xiaogu Huang, Jiao Chen, Jing Zhang, Lixi Wang, Q. Zhang, A new microwave absorber based on antimony-doped tin oxide and ferrite composite with excellent electromagnetic match, *Journal of Alloys and Compounds,* 506 (2010) 347-350.
20. Z. Zi, J. Dai, Q. Liu, H. Liu, X. Zhu, Y. Sun, Magnetic and microwave absorption properties of W-type $Ba(Zn_xCo_{1-x})_2Fe_{16}O_{27}$ hexaferrite platelets, *Journal of Applied Physics*, 109 (2011) 07E536.
21. Ali-Sharbati, Javad-Mola Verdi Khani, G.R. Amiri, R. Mousarezaei, Influence of dysprosium addition on the structural, morphological, electrical and magnetic properties of nano-crystalline W-type hexaferrites, *Bulliten of Materials Science,* 38 (2015) 1-5.
22. Y. Feng, T. Qiu, C. Shen, Absorbing properties and structural design of microwave absorbers based on carbonyl iron and barium ferrite, *Journal of Magnetism and Magnetic Materials,* 318 (2007) 8-13.
23. Xiaogu Huang, Jing Zhang, Hongzhou Wang, Shaoteng Yan, Lixi Wang, Z. Zhang, Er^{3+}-substituted W-type barium ferrite: preparation and electromagnetic properties, *Journal of Rare Earths,* 28 (2010) 940-943.
24. L. Wang, J. Song, Q. Zhang, X. Huang, N. Xu, The microwave magnetic performance of Sm^{3+} doped BaCo2Fe16O27, *Journal of Alloys and Compounds,* 481 (2009) 863-866.
25. C.A. Stergiou, G. Litsardakis, Electromagnetic properties of Ni and La doped strontium hexaferrites in the microwave region, *Journal of Alloys and Compounds*, 509 (2011) 6609-6615.
26. G. Albanese, E. Calabrese, A. Deriu, F. Licci, Mössbauer investigation of W-type hexaferrite of composition $BaZn_{2-x}Co_xFe_{16}O_{27}$, *Hyperfine Interactions*, 28 (1986) 487-489.
27. A. Paoluzi, F. Licci, O. Moze, G. Turilli, A. Deriu, G. Albanese, E. Calabrese, Magnetic, Mössbauer, and neutron diffraction investigations of W-type hexaferrite $BaZn_{2-x}Co_xFe_{16}O_{27}$ single crystals, *Journal of Applied Physics*, 63 (1988) 5074-5080.
28. G. Asti, F. Bolzoni, F. Licci, M. Canali, First order magnetization processes in uniaxial crystals: $(Zn,Co)_2BaFe_{16}O_{27}$, *IEEE Transactions on Magnetics*, MAG-14 (1978) 883-885.
29. D. Samaras, A. Collomb, S. Hadjivasiliou, C. Achilleos, J. Tsoukalas, J. Pannetier, J. Rodriguez, The rotation of the magnetization in the $BaCo_2Fe_{16}O_{27}$ W-type hexagonal ferrite, *Journal of Magnetism and Magnetic Materials*, 79 (1989) 193-201.
30. Sami H. Mahmood, Qusai Al Sheyab, Ibrahim Bsoul, Osama Mohsen, A.M. Awadallah, Structural and magnetic properties of Ga-substituted Co_2-W hexaferrites, *Current Applied Physics*, 18 (2018) 2590-2598.
31. C. Stergiou, G. Litsardakis, Preparation and magnetic characterization of Co^2-W strontium hexaferrites doped with Ni and La, *Journal of Magnetism and Magnetic Materials*, 323 (2011) 2362-2368.
32. Y.J. Yang, F. Wang, J. Shao, D. Huang, X. Liu, S. Feng, M. Wan, Q. Cao, Structural and magnetic properties of $Sr_{1-x}La_xFe_{12-x}(Cu_{0.5}Co_{0.5})xO_{19}$ hexaferrites prepared by the solid-state reaction method, *Bulliten of Materials Science,* 39 (2016) 119-123.
33. A. Awadallah, S.H. Mahmood, Y. Maswadeh, I. Bsoul, A. Aloqaily, Structural and magnetic properties of Vanadium Doped M-Type Barium Hexaferrite ($BaFe_{12-x}V_xO_{19}$), IOP Conference Series: *Materials Science and Engineering*, 92 (2015) 012006.
34. G.H. Dushaq, S.H. Mahmood, I. Bsoul, H.K. Juwhari, B. Lahlouh, M.A. AlDamen, Effects of molybdenum concentration and valence state on the structural and magnetic

properties of $BaFe_{11.6}Mo_xZn_{0.4-x}O_{19}$ hexaferrites, *Acta Metallurgica Sinica* (English Letters), 26 (2013) 509-516.

35. A. Collomb, P. Wolfers, X. Obradors, Neutron diffraction studies of some hexagonal ferrites: $BaFe_{12}O_{19}$, $BaMg_2$-W and $BaCo_2$-W, *Journal of Magnetism and Magnetic Materials,* 62 (1986) 57-67.
36. R.D. Shannon, Revised effective ionic radii and systematic studies of interatomic distances in halides and chalcogenides, *Acta Crystallographica A*, 32 (1976) 751-767.
37. B.E. Warren, X-ray Diffraction, Addison-Wesley, Reading, Massachsetts, 1969.
38. S.H. Mahmood, A. Awadallah, Y. Maswadeh, I. Bsoul, Structural and magnetic properties of Cu-V substituted M-type barium hexaferrites, IOP Conference Series: *Materials Science and Engineering,* 92 (2015) 012008.
39. B.D. Cullity, C.D. Graham, Introduction to magnetic materials, 2nd ed., John Wiley & Sons, Hoboken, NJ, 2011.
40. R. Grössinger, A critical examination of the law of approach to saturation I. fit procedure, *Physica Status Solidi* (a), 66 (1981) 665-674.
41. M.J. Iqbal, R.A. Khan, S. Mizukami, T. Miyazaki, Mössbauer and magnetic study of Mn, Zr and Cd substituted W-type hexaferrites prepared by co-precipitation, *Materials Research Bulletin,* 46 (2011) 1980-1986.
42. M.J. Iqbal, R.A. Khan, S. Mizukami, T. Miyazaki, Tailoring of structural, electrical and magnetic properties of $BaCo_2$W-type hexaferrites by doping with Zr–Mn binary mixtures for useful applications, *Journal of Magnetism and Magnetic Materials,* 323 (2011) 2137-2144.
43. I. Khan, I. Sadiq, M.N. Ashiq, Role of Ce–Mn substitution on structural, electrical and magnetic properties of W-type strontium hexaferrites, *Journal of Alloys and Compounds,* 509 (2011) 8042-8046.
44. J. Tang, X. Liu, K.M.U. Rehman, D. Li, M. Li, Y. Yang, Microstructure and characterization of W-type hexaferrite $Ba_{1-x}La_xFe_2^{2+}Fe_{16}^{3+}O_{27}$ prepared by solid state method, *Journal of Magnetism and Magnetic Materials,* 452 (2018) 354-359.
45. F. Guo, X. Wu, G. Ji, J. Xu, L. Zou, S. Gan, Synthesis and Properties Investigation of Non-equivalent Substituted W-Type Hexaferrite, *Journal of Superconductivity and Novel Magnetism*, 27 (2014) 411-420.
46. T. Tsutaoka, N. Koga, Magnetic phase transitions in substituted barium ferrites $BaFe_{12-x}(Ti_{0.5}Co_{0.5})xO_{19}$ (x = 0–5), *Journal of Magnetism and Magnetic Materials,* 325 (2013) 36-41.
47. S.H. Mahmood, M.D. Zaqsaw, O.E. Mohsen, A. Awadallah, I. Bsoul, M. Awawdeh, Q.I. Mohaidat, Modification of the magnetic properties of Co_2Y hexaferrites by divalent and trivalent metal substitutions, *Solid State Phenomena*, 241 (2016) 93-125.